Study of lifetime and phase transition in neutron-rich ^{98,100,102}Zr

S. Ansari,[1,2] J.-M. Régis,[1] J. Jolie,[1] N. Saed-Samii,[1] N. Warr,[1] W. Korten,[2] M. Zielińska,[2] M.-D. Salsac,[2] A. Blanc,[3] M. Jentschel,[3] U. Köster,[3] P. Mutti,[3] T. Soldner,[3] G.S. Simpson,[4] F. Drouet,[4] A. Vancraeyenest,[4] G. de France,[5] O. Stezowski,[6] C.A. Ur,[7] W. Urban,[8] P.H. Regan,[9,10] Zs. Podolyák,[9] C. Larijani,[9,10] C. Townsley,[9] R. Carroll,[9] E. Wilson,[9] H. Mach,[11,*] L.M. Fraile,[12] V. Paziy,[12] B. Olaizola,[12] V. Vedia,[12] A.M. Bruce,[13] O.J. Roberts,[13] J.F. Smith,[14] M. Scheck,[14] T. Kröll,[15] A.-L. Hartig,[15] A. Ignatov,[15] S. Ilieva,[15] S. Lalkovski,[16] N. Mărginean,[17] T. Otsuka,[18,19,20,21] N. Shimizu,[18] T. Togashi,[18] and Y. Tsunoda[18]

[1]*Institut für Kernphysik der Universität zu Köln, Zülpicher Str. 77, 50937 Köln, Germany*
[2]*Irfu, CEA, Université Paris-Saclay, F-91191 Gif-sur-Yvette, France*[†]
[3]*Institut Laue-Langevin, 71 avenue des Martyrs, 38042 Grenoble Cedex, France*
[4]*LPSC, 53 avenue des Martyrs, 38026 Grenoble Cedex, France*
[5]*Grand Accélérateur National d'Ions Lourds (GANIL), CEA/CRF-CNRS/IN2P3, 14076 Caen Cedex 05, France*
[6]*IPN de Lyon, 4, Rue Enrico Fermi, 69622 Villeurbanne Cedex, France*
[7]*INFN, via Marzolo 8, 35131 Padova, Italy*
[8]*Faculty of Physics, University of Warsaw, ul. Hoża 69, PL-00-681 Warsaw, Poland*
[9]*Department of Physics, University of Surrey, Guildford GU2 7XH, United Kingdom*
[10]*National Physical Laboratory, Teddington, Middlesex, TW11 0LW, United Kingdom*
[11]*National Centre for Nuclear Research, ul. Hoża 69, Warsaw, Poland*
[12]*Grupo de Fisica Nuclear, FAMN, Universidad Complutense, 28040 Madrid, Spain*
[13]*SCEM, University of Brighton, Lewes Road, Brighton, BN2 4GJ, United Kingdom*
[14]*School of Engineering, University of the West of Scotland, Paisley, PA1 2BE, United Kingdom*
[15]*Institut für Kernphysik, TU Darmstadt, Schlossgartenstr. 9, 64289 Darmstadt, Germany*
[16]*Faculty of Physics, University of Sofia, 1164 Sofia, Bulgaria*
[17]*Horia Hulubei NIPNE, 77125 Bucharest, Romania*
[18]*Center for Nuclear Study, University of Tokyo, Hongo, Bunkyo-ku Tokyo 113-0033, Japan*
[19]*Department of Physics, University of Tokyo, Hongo, Bunkyo-ku Tokyo 113-0033, Japan*
[20]*NSCL, Michigan State University, East Lansing, Michigan 48824, USA*
[21]*Instituut voor Kern- en Stralingsfysica, KU Leuven, B-3001 Leuven, Belgium*

(Dated: July 10, 2017)

Rapid shape changes are observed for neutron-rich nuclei with a mass around A=100. In particular, a sudden onset of deformation is observed in the Zr and Sr isotopic chains at N=60: low-lying states in N≤58 nuclei are nearly spherical, while those with N≥60 have a rotational character. Nuclear lifetimes as short as few ps can be measured using fast-timing techniques with $LaBr_3$(Ce)-scintillators, yielding a key ingredient in the systematic study of the shape evolution in this region. We used neutron-induced fission of ^{241}Pu and ^{235}U to study lifetimes of excited states in fission fragments in the A∼100 region with the EXILL-FATIMA array located at the PF1B cold neutron beam line at the Institut Laue-Langevin. In particular, we applied the generalized centroid difference method to deduce lifetimes of low-lying states for the nuclei ^{98}Zr (N=58), ^{100}Zr and ^{102}Zr (N≥60). The results are discussed in the context of the presumed phase transition in the Zr chain by comparing the experimental transition strengths with the theoretical calculations using the interacting boson model and the Monte Carlo Shell Model.

PACS numbers: 21.60.Fw, 21.10.Re, 21.60.Ev, 27.80+w

I. INTRODUCTION

The last few decades have seen a focus on the shape-phase transition in nuclei around A=100. The appearance of quadrupole deformation beyond N=60 in the A∼100 mass region was discovered in the 1960's by S.A.E. Johansson [1] in a study of γ rays emitted by fission fragments. Soon after, Cheifetz et al [2] observed regular rotational bands in neutron-rich Zr, Mo, Ru and Pd isotopes populated in spontaneous fission of ^{252}Cf. In particular, the lifetimes of 2_1^+ states in ^{100,102}Zr obtained in that study [2] confirmed their highly-deformed character. These experimental discoveries triggered an important theoretical effort to explain the origin of quadrupole deformation in A∼100 nuclei; early calculations are described for example in Refs. [3, 4].

The simplest estimate of nuclear deformation can be obtained from the energy of the 2_1^+ state in even-even nuclei. For Sr (Z=38) and Zr (Z=40) isotopes it is observed to decrease dramatically at N=60, while the evolution is much more gradual in Mo nuclei (Z=42) (see Fig. 1). A gradual decrease of the 2_1^+ energy is also observed for ^{92,94,96}Kr nuclei (Z=36). Judging by level energies alone, the Z-boundaries of the region of the shape transition at N=60 seem to be clearly defined [5]. This is consistent with the results of mass measure-

* Deceased
† saba.ansari@cea.fr

ments for ^{96,97}Kr [6] that show a smooth evolution towards the dripline in contrast to the sharp changes observed for heavier N=60 nuclei. It should be noted here that a recent study reported a significant drop in energy for ^{98}Kr, and further stabilized for ^{100}Kr [5], which suggests that a shape transition may appear in the Kr isotopic chain at N=62 instead of N=60.

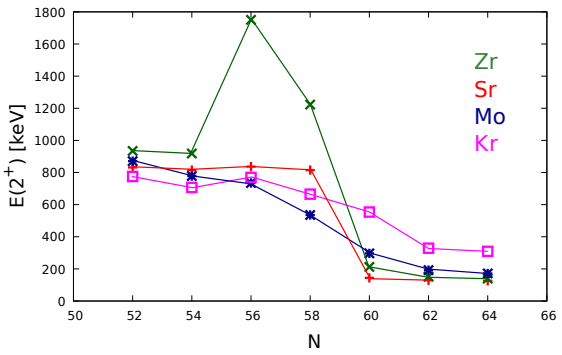

FIG. 1. Evolution of the 2_1^+ excitation energy as a function of neutron number in the A ~ 100 region. The transition energies are taken from National Nuclear Data Center [7] and the recent results for ^{98,100}Kr are adopted from Ref. [5]

The $R_{4/2} = E(4_1^+)/E(2_1^+)$ ratios for N≥60 Sr, Zr, Mo and Ru nuclei have a value around 3 [2], which is expected for a rigid rotor and is consistent with a static character of the deformation in this mass region. Again, a very different behavior has recently been observed for the 4^+ state in ^{96}Kr, with the $R_{4/2}$ value dropping abruptly to 2.1, suggesting a dynamical character of the deformation [8].

A similar picture is emerging from measurements of transition probabilities. A Coulomb excitation study of ^{96}Kr [9] yielded a B(E2; $2_1^+ \longrightarrow 0_1^+$) value much lower than those for ^{98}Sr and ^{100}Zr, and only slightly higher than that for ^{94}Kr [9]. In contrast, regular rotational ground-state bands were observed in ^{97,99}Rb [10], and the obtained transition probabilities show that the deformation of these nuclei is essentially the same as that observed inside the well-deformed region, thus establishing ^{97}Rb as its cornerstone. Recent lifetime measurements for ^{99,101}Y and ^{101,103,105}Nb [11] confirmed that these nuclei are as deformed as the neighboring even-even isotopes with N≥60.

Sudden shape changes may be interpreted as a result of an inversion of two distinct configurations associated with different nuclear shapes. Indeed, the shape transition at N=60 is accompanied by the appearance of low-lying 0_2^+ states indicating possible shape coexistence [12] and, similar to the 2_1^+ state, an abrupt drop of the 0_2^+ energy is observed at N=60. The recent Coulomb excitation study of ^{96,98}Sr [13, 14] provided firm evidence for configuration inversion in these nuclei, demonstrating important similarities in terms of transition probabilities and spectroscopic quadrupole moments between the ground-state band in ^{96}Sr and the structure built on the 0_2^+ state in ^{98}Sr. These conclusions are consistent with the results of a new lifetime measurement in the Sr isotopic chain [15]. The interpretation of $E2$ matrix elements obtained in the Coulomb excitation measurement [13, 14] using the two-state mixing model points to very low mixing between prolate and spherical configurations in the wave functions of the 0^+ states in ^{98}Sr, in spite of their proximity in energy. The same conclusion can be drawn from the measured $E0$ transition strength between the 0_2^+ and 0_1^+ states in ^{98}Sr [16, 17] and also from $E0$ and $E2$ transition strengths in ^{100}Zr [18–20]. The weak mixings of the coexisting structures in ^{98}Sr and ^{100}Zr are very different from those observed for other regions of shape coexistence, for example in ^{74,76}Kr [21] and $^{182-188}$Hg [22] isotopes, where strong mixing makes the change of the ground state properties more gradual.

The local character of the shape change suggests that specific proton and neutron orbitals are responsible for this effect. Unfortunately, the valence space required to describe A~100 nuclei is currently too large for conventional shell model calculations, although they could correctly describe the properties of light (N<60) Zr isotopes [23]. However, recent advances with Monte Carlo Shell Model have made it possible to investigate the origin of the shape transition at N=60 [24] and relate it to the strong proton-neutron interaction between proton $\pi 1g_{9/2}$ and neutron $\nu 1g_{7/2}$ subshells. Promotion of protons from the $\pi 2p_{1/2}$ to the $\pi 1g_{9/2}$ orbital causes the reduction in the spin-orbit coupling for neutron orbitals, reducing the $\nu 2d_{5/2}$ - $\nu 1g_{7/2}$ gap. Increased occupation of the $\nu 1g_{7/2}$ orbital leads in turn to an increase in spin-orbit splitting in the proton sector and reduction of the $\pi 2p_{1/2}$ - $\pi 1g_{9/2}$ gap. This self-reinforcing effect, known as type-II shell evolution [25], is suggested to be responsible for appearance of deformed states in Zr isotopes. Since these specific particle-hole excitations lead to a significant reorganization of the effective single-particle energies, the mixing of normal states and those with deformation-optimized shell structure is suppressed, consistent with experimental results. The calculations of Togashi et al. [24] predict a dramatic shape change between the ground states of ^{98}Zr and ^{100}Zr, with the 0_2^+ in ^{98}Zr becoming the 0_1^+ state of ^{100}Zr and the ground state of ^{98}Zr becoming the non-yrast 0_2^+ state in ^{100}Zr and beyond.

The current paper presents new experimental results on lifetimes in neutron-rich Zr isotopes, which bring systematic information on evolution of nuclear deformation and collectivity in the vicinity of the N=60 shape transition. The measured transition strengths are compared to the results of Monte Carlo Shell Model and IBM(1) calculations in order to get a better understanding of the shape transition and configuration inversion in the Zr isotopic chain.

II. EXPERIMENT

Lifetimes of low-lying excited states of ^{98,100,102}Zr have been measured through a prompt-fission spectroscopy experiment performed at the Institut Laue-Langevin (ILL) Grenoble, France. In this experiment, the high-flux cold neutron beam at PF1B [26] was inducing the fission reaction on targets of ^{235}U and ^{241}Pu. The EXILL-FATIMA setup consisted of 8 EXOGAM clovers and 16 $LaBr_3$ detectors, which were placed at a distance of 14.5 cm and 8.5 cm, respectively, from the

target [27]. Each of the targets was sandwiched between Be layers to stop the fission fragments. The $LaBr_3$ detectors were arranged in a compact configuration to maximize the number of $\gamma-\gamma$ coincidences. A detailed description of the collimation of the neutron beam can be found in Ref. [28], the detector arrangement and analogue fast-timing electronics in Ref. [27] and the trigger-less data acquisition system in Ref. [29].

A. Data analysis

The data were sorted using a C++ based software, SOCOv2 [30], developed in the Institute of Nuclear Physics, Cologne. For the present application, coincidences between exactly one clover (after add-back) and two $LaBr_3$ detector were required within the 120 ns time window, meaning the γ-ray multiplicity was equal to three. This condition reduced the size of the original data set by a few orders of magnitude. The modern fast-timing method of Mirror Symmetric Centroid Difference (MSCD) [31] was used in the present work for lifetime determination. By using the feeding transition (resp. decay) of a sequential $\gamma-\gamma$ cascade as the start signal of a TAC module and the decay (resp. feeding transition) as the stop, we observed a signal delayed (resp. anti-delayed) by the lifetime τ of the decaying state. The centroid of the resulting TAC spectrum is thus shifted by τ (resp. -τ) from its prompt position. The MSCD method is based on the difference between the centroids of these two independent time distributions of a sequential $\gamma-\gamma$ cascade. This method considers the centroid difference as a physical observable and as the name suggests, interprets the centroid difference of the $\gamma-\gamma$ cascade as mirror symmetric with respect to a start-stop inversion, or equivalently, to a hypothetical inversion of the transitions in the cascade. The MSCD method in case of no background is described by the following equation:

$$\begin{aligned}\triangle C(E_{feeder}, E_{decay}) &= C_{delayed} - C_{anti-delayed} \\ &= C^{D}(E_{feeder}, E_{decay}) - C^{AD}(E_{decay}, E_{feeder}) \\ &= PRD(E_{feeder}, E_{decay}) + 2\tau, \end{aligned} \quad (1)$$

where C^D describes the centroid of the delayed time distribution and C^{AD} is the centroid of anti-delayed one. The PRD is the Prompt Response Difference which describes the combined $\gamma-\gamma$ time-walk of the setup. The PRD for two γ-ray energies in a $\gamma-\gamma$ cascade is given as:

$$PRD(E_{feeder}, E_{decay}) = PRD(E_{feeder}) - PRD(E_{decay}), \quad (2)$$

$$\begin{aligned}PRD(E_{feeder}, E_{decay}) &= PRD_{E_{decay}}(E_{feeder}) \\ &= -PRD_{E_{feeder}}(E_{decay}) \end{aligned} \quad (3)$$

where $PRD_{E_{decay}}(E_{feeder})$ [$PRD_{E_{feeder}}(E_{decay})$] is the Prompt Response Difference at the feeding (decay) transition when the reference energy is at the decay (feeding) transition. This shows the mirror symmetry of the method in which both PRD and centroid difference are mirror symmetric.

In the present case the PRD curve is plotted for E_{ref} = 344 keV (i.e., the value of the PRD at 344 keV is 0 ps) by using the following calibration equation:

$$PRD(E_\gamma) = \frac{a}{\sqrt{b+E_\gamma}} + cE_\gamma + d(E_\gamma)^2 + e, \quad (4)$$

where a, b, c, d and e are the fit parameters. The uncertainty on the PRD was obtained from the fit residuum (mean root squared derivation) and is equal to δ(PRD) = 10 ps for the 3σ limit. The PRD curve (shown in Fig. 2) can be used to read the PRD value for any sequential $\gamma-\gamma$ cascade within the energy range of 0 – 1400 keV. The determination of the timing uncertainties and the PRD calibration procedure of the EXILL-FATIMA setup are described in detail in [27].

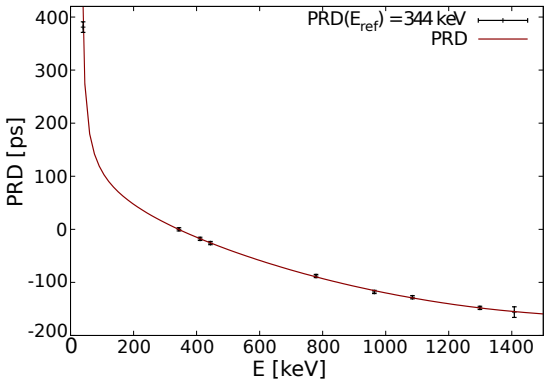

FIG. 2. PRD curve obtained using a ^{152}Eu source.

The MSCD method has been extended to the Generalized Centroid Difference Method (GCDM) for the system of N nearly identical fast-timing detectors, as in the case of the EXILL-FATIMA campaign. In this method, instead of evaluating individual centroid differences for '$C_{start,stop}$' between two independent timing distributions, the superimposed TAC spectrum of all the combinations of 'start, stop' belonging to the N-detector system is evaluated [32]. Similar to equation 1, the relation between the mean centroid difference ($\overline{\triangle C(E_\gamma)}$) and the mean Prompt Response Difference ($\overline{PRD}$) is given by:

$$\overline{\triangle C_{FEP}} = \overline{PRD} + 2\tau, \quad (5)$$

where FEP stands for full-energy peak. Equation 5 is valid if the time differences between the start and the stop events are statistically distributed around the mean $\overline{\triangle C_{FEP}}$ or $\overline{PRD}$, and are independent of the detector-detector combination.

B. Lifetime determination

We have measured the lifetimes of the 2_1^+ and 4_1^+ states of ^{98}Zr and 2_1^+, 4_1^+ and 6_1^+ states of ^{100,102}Zr, analyzing the data collected with each of the targets (^{235}U and ^{241}Pu) separately. We present the details of the analysis procedure using the examples of 2_1^+ and 4_1^+ states of ^{100,102}Zr.

The most prominent source of background in the low-energy range ($\leq$ 300 keV) for the EXILL-FATIMA setup was the Compton scattering. It arises from the superposition of Compton continua of multiple γ rays produced in the fission process. In an ideal setup, Eq. 5 can be used for lifetime determination, however, in a real setup the experimental centroid difference ($\triangle C_{exp}$) must be corrected in order to account for the Compton background ($\triangle C_{BG}$), following:

$$\triangle C_{FEP} = \triangle C_{exp} + \frac{\triangle C_{exp} - \triangle C_{BG}}{p/b}, \tag{6}$$

where, p/b is the peak to background ratio. Equation 6 can be used for the Compton background correction when only one background component is present [27, 31]. However, since two FEP's (feeder and decay) are used in the lifetime analysis, the Compton background underneath each of the FEP's in the γ-γ cascade must be considered separately [15]:

$$\triangle C_{FEP} = \triangle C_{exp} + \frac{1}{2}\Big[t_{corr.}(feeder) + t_{corr.}(decay)\Big], \tag{7}$$

where,

$$t_{corr.}(feeder) = \Big[\frac{(\triangle C_{exp} - \triangle C_{BG})}{p/b}\Big]_{feeder},$$
$$t_{corr.}(decay) = \Big[\frac{(\triangle C_{exp} - \triangle C_{BG})}{p/b}\Big]_{decay}, \tag{8}$$

and

$$\tau = \frac{1}{2}(\triangle C_{FEP} - PRD) \tag{9}$$

In Eqs. 7 and 9, $\triangle C_{exp}$ is the experimental value, $\triangle C_{FEP}$ is the one related to FEP events only, corrected for the contribution of the Compton background ($\triangle C_{BG}$). The term $t_{corr.}$(feeder) (resp. $t_{corr.}$(decay)) in Eq. 8 is the background correction resulting from the feeding (decay) transition in a spectrum gated on the decay (feeding) transition, and hence at the reference energy (E_{ref}). When estimating the uncertainty on the lifetime, the individual contributions are taken into account as follows:

$$\delta\tau = \frac{1}{2}\sqrt{\delta \triangle {C_{exp}}^2 + \delta {t_{corr.}}^2 + \delta PRD^2}, \tag{10}$$

where $\delta t_{corr.}$ corresponds to the mean uncertainty of the two Compton background correction terms.

The high multiplicity of γ rays produced in the fission process can sometimes lead to erroneous results. For example, the transitions of interest (feeder and decay) for the lifetime measurements of 4^+ and 6^+ states of ^{100,102}Zr lie in the same energy range (480-500 keV) as the low-lying γ-ray transitions in ^{138}Xe. ^{138}Xe is one of the possible complementary partners of both ^{100}Zr and ^{102}Zr in the ^{241}Pu fission, through:

$$^{241}_{94}\mathrm{Pu} + n_{th} \longrightarrow {}^{102}_{40}\mathrm{Zr}_{62} + {}^{138}_{54}\mathrm{Xe},\ 2n \text{ emission}$$
$$^{100}_{40}\mathrm{Zr}_{62} + {}^{138}_{54}\mathrm{Xe},\ 4n \text{ emission}.$$

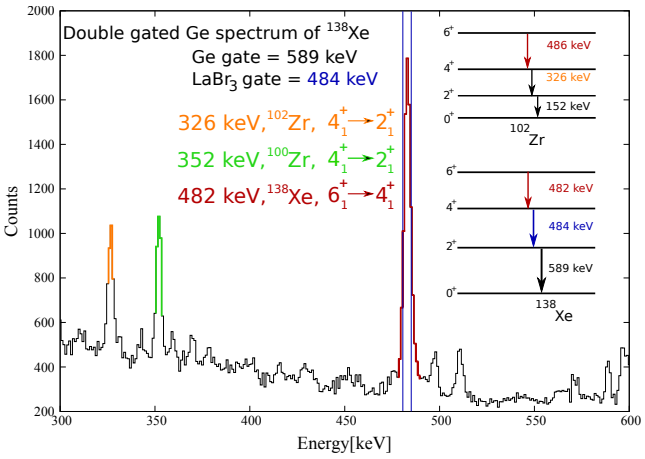

FIG. 3. The double-gated spectrum of ^{138}Xe being a complementary partner of ^{100}Zr and ^{102}Zr. Prominent peaks in the spectrum (shown in different color) correspond to transitions in ^{100}Zr, ^{102}Zr and ^{138}Xe.

This is illustrated by Fig. 3 showing a double-gated (Ge + $LaBr_3$) spectrum of ^{241}Pu fission products, gated on two transitions in ^{138}Xe: $2^+ \longrightarrow 0^+$ (589 keV) observed with the Ge detectors and $4^+ \longrightarrow 2^+$ (484 keV) with $LaBr_3$ detectors. In addition to prominent γ rays in ^{138}Xe, one can see also γ rays (highlighted in Fig. 3) originating from ^{100,102}Zr, proving that ^{138}Xe and ^{100,102}Zr are complementary partners and that the lifetime measurements involving those particular transitions may be biased. This is, however, not the case for the fission of ^{235}U, and thus the lifetimes of 4^+, 6^+ state of ^{100,102}Zr can be correctly determined from this latter data set.

1. ^{98}Zr

Lifetimes for ^{98}Zr were investigated for the 2^+_1 and the 4^+_1 states. The lifetime analysis for the 2^+ state is done by using the 1223 keV $2^+ \longrightarrow 0^+$ transition depopulating this state as a stop and that feeding it (621 keV, $4^+ \longrightarrow 2^+$) as a start. The latter is used as the reference for the PRD. In addition, a gate on Ge singles is applied on the $6^+ \longrightarrow 4^+$ transition at 647 keV to select the cascade of interest and to improve the peak-to-background ratio. The correction for Compton background that lies underneath the peak of interest is applied using Eq. 7. Due to low statistics obtained for both fission targets, and short lifetimes, only upper limits could be determined.

2. ^{100}Zr

The lifetimes of the 2^+ and 4^+ states of ^{100}Zr were determined using GCDM as explained in Sec. II A. In addition, the slope method was also used to extract the 2^+ lifetime, as shown in Fig. 4. The spectra in Fig. 4(b), in contrast to those in Fig. 4(a), display two slope components, a fast (small bump at the beginning) and a slow one. Especially for lifetimes be-

low 1 ns, it is difficult to distinguish between the two slope components and select the time range in which only the slow slope component will be fitted. The different precision on the lifetime obtained using data from each of the fission targets is due to a better peak-to-background ratio in the ^{235}U data.

For comparison, if we try to apply Eq. 9 to $\triangle C_{exp}$ values from Fig. 4 in order to extract the lifetime assuming no background, we obtain significantly different values (603(11) ps for ^{235}U target and 509(9) ps for ^{241}Pu) from those extracted using the slope method. This demonstrates that also for lifetimes below 1 ns the correction for Compton background should be performed, and consequently we further apply GCDM with its reliable background correction procedure to the 2_1^+ state of ^{100}Zr.

Fig. 5 illustrates the complete GCDM procedure for the lifetime evaluation of the 2^+ state of ^{100}Zr with ^{241}Pu as a fission target. Fig. 5(a) presents the double-gated (Ge + $LaBr_3$) spectrum with E_{ref} of 352 keV (transition feeding the 2^+ state) and FEP is the decay of the 2^+ state at E=212 keV. A narrow energy gate of 6 keV is applied on the FEP and the two centroids of independent delayed and anti-delayed time distributions are calculated. The difference between these two time distribution centroids yields the $\triangle C_{exp}$ value. The Compton background correction is performed by: 1) finding the time distribution of the background through gating on a few background points in the vicinity of the FEP using the same channel width (6 channels), 2) plotting the centroid difference of these background points against their respective energy, 3) fitting this dependence using a polynomial function, and 4) reading the $\triangle C_{BG}$ at the position of the FEP from the thus obtained background curve (as shown in Fig. 5(c)). The PRD correction is directly read from the PRD curve in Fig. 5(c). This curve is shifted with respect to the original plot (see Ref. [27]) in order to yield PRD equal to 0 at E_{ref} of 212 keV.

The same procedure is repeated with the feeding and depopulating transitions interchanged (E_{ref} at 352 keV and FEP at 212 keV). In this case, the background region is different and consequently different background gates are applied. It should be noted that the PRD curve as well as the Compton background correction curve in Fig. 5(d) are inverted with respect to those in Fig. 5(c) since the E_{ref} is flipped from the transition feeding the state of interest to that depopulating it. Equations 7 and 9 are then applied to the values listed in Figs. 5(c) and 5(d) yielding the lifetime of $\tau_2^+ = 830(30)$ ps.

3. ^{102}Zr

The lifetime of the 2^+ state of ^{102}Zr was determined using the slope method on data obtained from both targets. Fig. 6 shows the time distribution observed with the ^{241}Pu target. The slow component of the slope is more prominent compared to that observed for ^{100}Zr (Fig. 4) because of the longer lifetime of the 2^+ state of ^{102}Zr and a relatively low background contribution to the peak. Consistent values were obtained for both targets: 2.91(15) ns for ^{241}Pu and 2.9(2) ns for ^{235}U.

To determine the previously unknown lifetimes of the 4_1^+ and 6_1^+ states, the GDCM was applied to the data collected

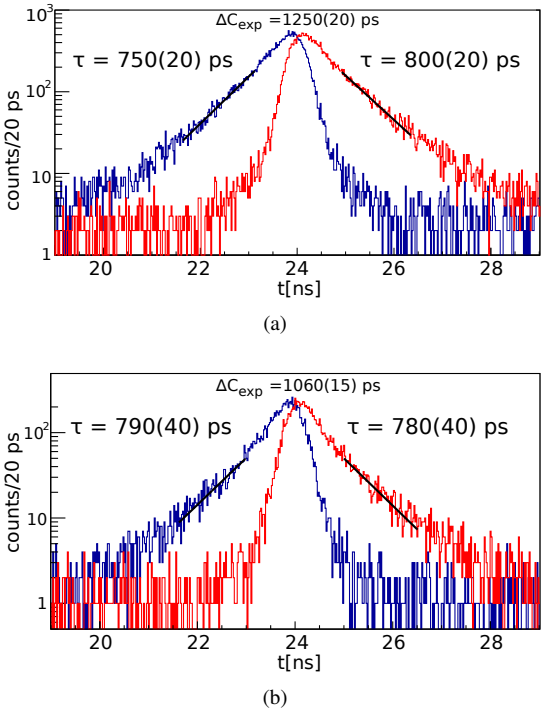

FIG. 4. Lifetime determination using the slope method for the 2_1^+ state of ^{100}Zr. The top panel (a) displays delayed (in red) and anti-delayed (in blue) time distribution of the state of interest from ^{235}U fission, and the bottom panel (b) from ^{241}Pu fission.

using both ^{235}U and ^{241}Pu targets. The lifetime analysis for the 4^+ state of ^{102}Zr using the ^{235}U target data is presented in Figs. 7 and 8. It follows the same procedure as for ^{100}Zr except that in this case the centroid difference related to the Compton background ($\triangle C_{BG}$) is fitted using a quadratic function. It is worth mentioning that for this state the background contribution was larger with respect to the FEP as was the $\triangle C_{BG}$ correction. The parallel adjustment of the PRD curve is made as per Eq. 2 in order to cross the energy axis at the reference energy. It should be noted that the PRD curve in Figs. 7(c) and 5(c) does not change its shape for different reference energies and only a parallel shift is observed, which is related to the $\gamma - \gamma$ time walk of the corresponding energies. The lifetimes obtained for the 4_1^+ and 6_1^+ states with the ^{241}Pu target are influenced by the presence in the γ-ray spectra by the transitions in the complementary fission partner ^{138}Xe, as explained in Sec. II B. This is, however, not the case for data collected with the ^{235}U fission target. A value of 46(7) ps was determined for the lifetime of the 4^+ state, using $t_{corr.}$(feeder) = 16(5) ps and $t_{corr.}$(decay) = −9(10) ps. For the 6_1^+ state, an upper limit of 12 ps was obtained.

III. RESULTS AND DISCUSSION

The obtained lifetimes are presented in Tab. I. Only upper limits could be determined for the 2^+ and 4^+ states of ^{98}Zr,

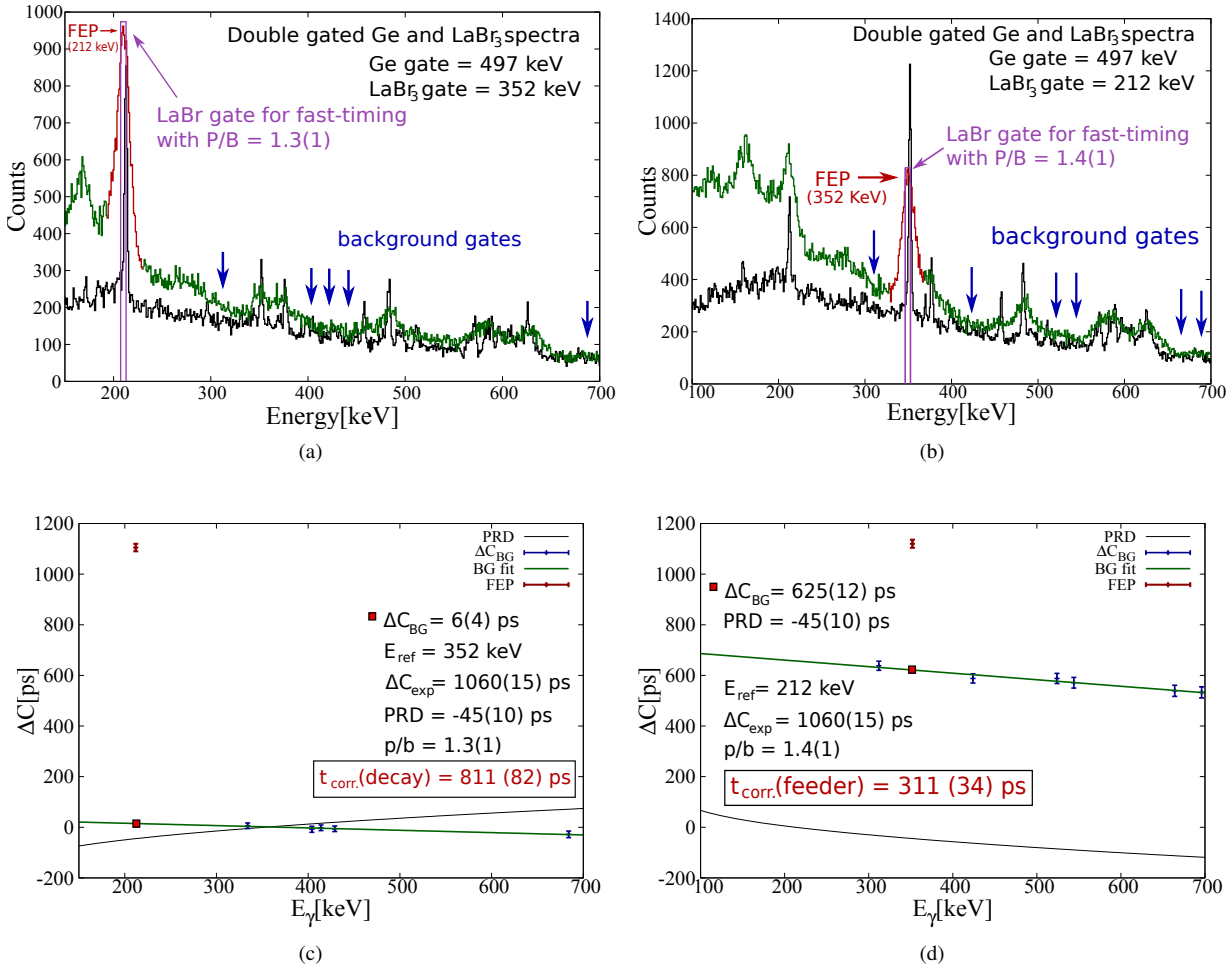

FIG. 5. Lifetime analysis for the 2_1^+ state in ^{100}Zr. Panels a) and b) show the double-gated Ge (shown in black) and $LaBr_3$ (green) spectra. Panels c) and d) display the Compton background correction procedure (see text for details).

and 6^+ state of ^{102}Zr, due to the low statistics, low peak-to-background ratios and short lifetimes. We concluded from the analysis performed for the 2^+ state of ^{100}Zr that the slope method is sensitive to background for lifetimes below 1 ns whereas the GCDM gives consistent results for both targets even though the peak-to-background ratio was dramatically different. The lifetimes of the 4^+ and 6^+ states of ^{100,102}Zr measured using the ^{241}Pu fission target are significantly different from those obtained with ^{235}U. This is related to the contamination of relevant γ-ray spectra by transitions in the complementary fission partner, as explained in Sec. II B.

Lifetimes in ^{98}Zr were previously measured in a $\beta-\gamma-\gamma$ experiment using the centroid shift method [33] and those in ^{100}Zr using the technique of time-integral perturbed angular correlations for long lived 2^+ state and the Doppler profile method for short-lived 4^+ and 6^+ states [34, 35]. These values are in good agreement with the present results as shown in Tab. I.

The present experimental lifetime results are used to calculate the B(E2) transition strengths and are compared with theoretical calculations using the Interacting Boson Model (IBM(1)) [36] and the Monte Carlo Shell Model (MCSM) [24], as shown in Fig. 9.

The IBM(1) calculations, described in detail in Ref. [36], used ^{90}Zr as the core. Good agreement with the present experimental results is found for ^{100,102}Zr. Since only upper limits are currently known for the lifetimes in ^{98}Zr, it is difficult to make firm conclusions on the evolution of transition probabilities from ^{98}Zr to ^{100}Zr which is predicted by the IBM(1) to be gradual. It should be noted that these calculations also predict a smooth change in energy with increasing neutron number, contrary to the experimental observations (see Fig. 1). In contrast, the dramatic decrease of the 2^+ level energy when going from ^{98}Zr to ^{100}Zr has been well reproduced by recent state-of-the-art MCSM calculation [24]. Unlike the conventional shell model calculations that are constrained by the size of the configuration space, the MCSM allows the calculation in large configuration spaces up to 3.7×10^{23}. Our data on ^{100,102}Zr agree very well with the MCSM predictions, while the obtained upper limit on the 2_1^+ lifetime in ^{98}Zr does not

TABLE I. Lifetimes of yrast states in ^{98,100,102}Zr extracted using fast-timing methods from the ^{241}Pu and ^{235}U data from the EXILL-FATIMA campaign. All values are given in ps unless mentioned otherwise. The literature values are the most recent values from National Nuclear Data Center [7] with the original reference provided. All the lifetime results are quoted with 1σ confidence limit except for 2^+ state of ^{102}Zr which is within a 2σ interval.

		Lifetime (τ)				
Nucleus	J^π	^{241}Pu	^{235}U	**adopted**	literature	B(E2; J→J-2)[e^{2}b^2] (adopted)
^{98}Zr	2^+	≤ 10	≤ 6	**≤6**	≤ 15 [33]	≥0.005
	4^+	≤ 20	≤ 15	**≤15**	29(9) [33]	≥0.06
^{100}Zr	2^+	830(30)	850(20)	**840(18)**	865(80) [34]	$0.210^{+0.005}_{-0.005}$
	4^+	25(10)[a]	37(4)	**37(4)**	54(4) [35]	$0.41^{+0.05}_{-0.04}$
	6^+		12(5)	**12(5)**	7.0(15) [35]	$0.22^{+0.16}_{-0.07}$
^{102}Zr	2+	2.91(15) ns	2.9(2) ns	**2.90(13) ns**	2.6(6) ns [34]	$0.282^{+0.014}_{-0.013}$
	4^+	21(15) [a]	46(7)	**46(7)**	-	$0.47^{+0.08}_{-0.06}$
	6^+	13(11) [a]	≤ 12	**≤12**	-	≥0.25

[a] The lifetimes determined from the ^{241}Pu data are affected by the contamination from γ-ray transitions in the complementary fission partner as explained in Sec. II B .

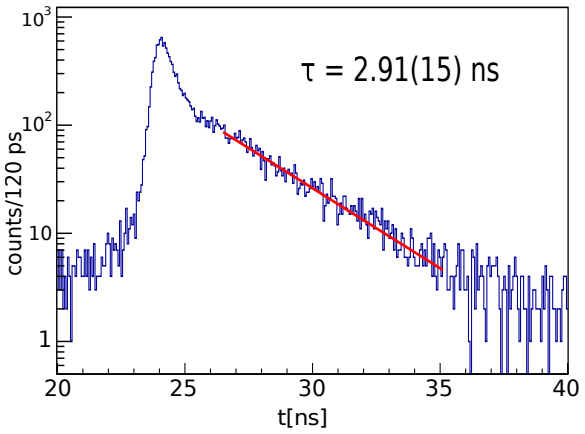

FIG. 6. Lifetime determination for the 2^+ state of ^{102}Zr using the ^{241}Pu target data. The independent anti-delayed time spectrum resulting from the FEP events is inverted and aligned before being summed to the delayed time distribution. The slope has been determined by fitting the data in the range from 25.5 ns to 35 ns and by slightly changing the fit region and the level of random background, deviation upto 2σ confidence interval was observed.

permit the discrimination between the drastic phase transition at N=60 predicted by MCSM and a smooth onset of collectivity as per the IBM(1). Our lower limit on the B(E2, $4^+_1 \rightarrow 2^+_1$) value in ^{98}Zr is not in agreement with the literature value, but is consistent with both the MCSM and IBM(1) calculations. The upper limit on the lifetime of the 6^+_1 state in ^{102}Zr does not allow for a meaningful comparison with the either model predictions. Definite lifetimes in ^{98}Zr are required that will provide the final verdict on the phase transition in this region and also allow us to further investigate the phenomenon of shape coexistence.

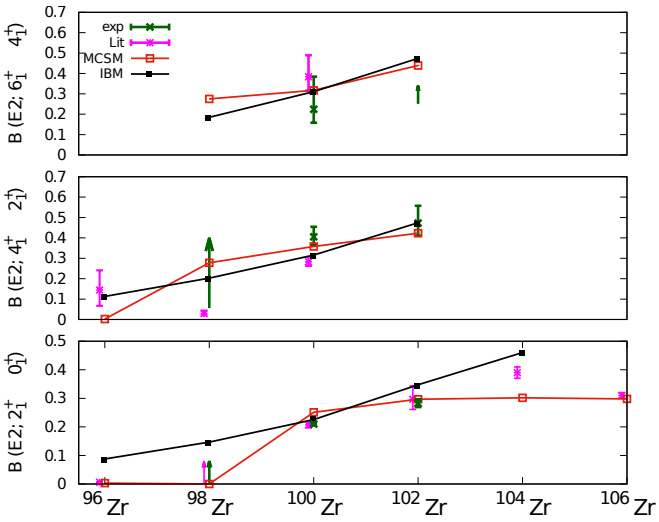

FIG. 9. Known B(E2; $2^+_1 \rightarrow 0^+_1$), B(E2; $4^+_1 \rightarrow 2^+_1$), B(E2; $6^+_1 \rightarrow 4^+_1$) values in ^{98,100,102}Zr, compared with the IBM(1) [36] and MCSM [24] calculations. The B(E2) values obtained in the present study (see Table I) are plotted in green and and the literature values [33–35] in magenta. All values are expressed in e^2b^2.

IV. SUMMARY

We studied lifetimes of yrast states in ^{98,100,102}Zr populated in neutron-induced fission of ^{241}Pu and ^{235}U using a combination of fast-timing $LaBr_3$ detectors and EXOGAM clovers. The lifetimes were determined using the slope method, applicable for the lifetimes above approximately 1 ns, and the

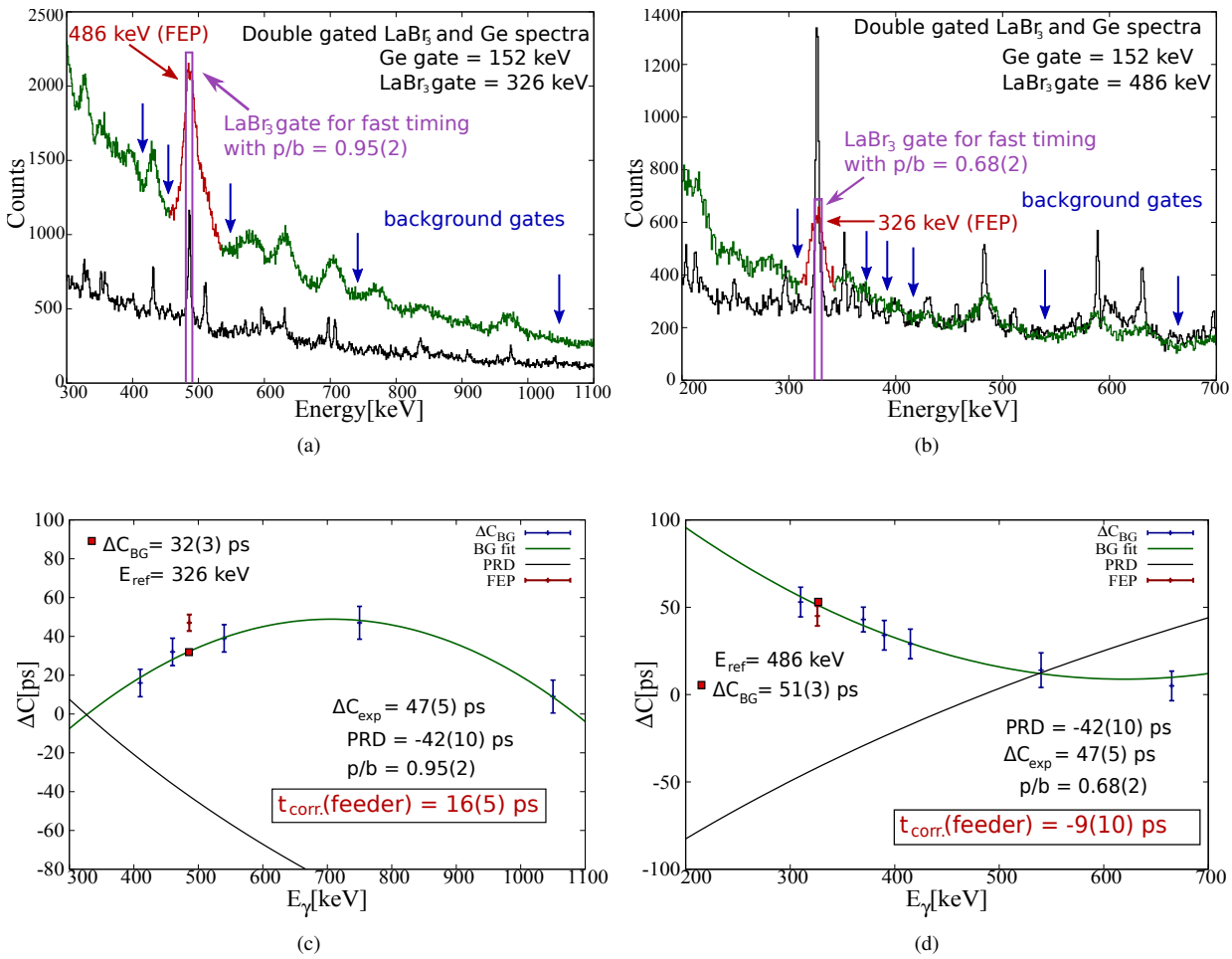

FIG. 7. Lifetime analysis for the 4^+ state in ^{102}Zr. Panels a) and b) display double-gated Ge (shown in black) and $LaBr_3$ (green) spectra. Panels c) and d) show the Compton background correction procedure (see text for details).

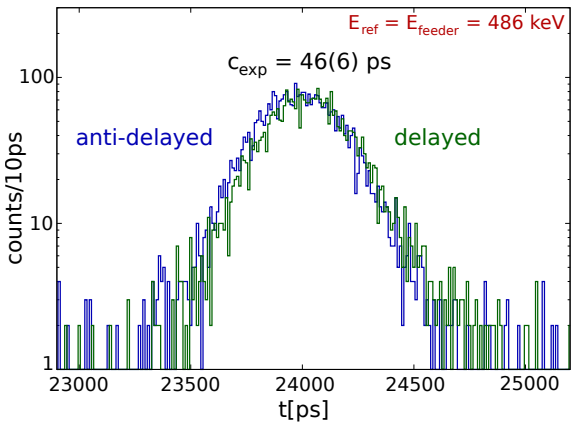

FIG. 8. Two independent time distributions (delayed and anti-delayed) for the 4^+ state of ^{102}Zr.

Generalized Centroid Difference Method for shorter lifetimes. The lifetime of the 4_1^+ state and an upper limit on the lifetime of the 6_1^+ state in ^{102}Zr were obtained for the first time. For other lifetimes determined in this study, good agreement was found with the literature values. The presently determined upper limits on the lifetimes in the ground-state band of ^{98}Zr do not permit conclusions on the possible shape phase transition in the Zr isotopic chain at N=60.

ACKNOWLEDGEMENTS

The EXILL&FATIMA campaign would not have been possible without the support of several services at the ILL and the LPSC. We are grateful to the EXOGAM collaboration for the loan of the detectors, to GANIL for assistance during installation and dismantling, and to the FATIMA collaboration for the provision of $LaBr_3$(Ce) detectors and analogue electronics. This work was supported by German BHBF under grant 05P15PKFNA and 05P12PKNUF. Theoretical studies including MCSM calculations were supported in part by JSPS Grants-in-Aid for Scientific Research (23244049), in part by HPCI Strategic Program (hp150224), in part by MEXT

and JICFuS and Priority Issue on Post-K computer (Elucidation of the fundamental laws and evolution of the universe) (hp160211), and by the CNS-RIKEN joint project for large-scale nuclear structure calculations.

[1] S. A. Johansson, Nuclear Physics **64**, 147 (1965).

[2] E. Cheifetz, R. C. Jared, S. G. Thompson, and J. B. Wilhelmy, Phys. Rev. Lett. **25**, 38 (1970).

[3] D. Arseniev, A. Sobiczewski, and V. Soloviev, Nuclear Physics A **139**, 269 (1969).

[4] R. Sheline, I. Ragnarsson, and S. Nilsson, Physics Letters B **41**, 115 (1972).

[5] F. Flavigny, P. Doornenbal, A. Obertelli, J.-P. Delaroche, M. Girod, *et al.*, Phys. Rev. Lett. **118**, 242501 (2017).

[6] S. Naimi, G. Audi, D. Beck, K. Blaum, C. Böhm, *et al.*, Phys. Rev. Lett. **105**, 032502 (2010).

[7] M. Wang, G. Audi, A. H. Wapstra, F. G. Kondev, M. MacCormick, X. Xu, and B. Pfeiffer, Chin.Phys.C **36**, 1603 (2012).

[8] J. Dudouet, A. Lemasson, G. Duchêne, M. Rejmund, E. Clément, C. Michelagnoli, F. Didierjean, *et al.*, Phys. Rev. Lett. **118**, 162501 (2017).

[9] M. Albers, N. Warr, K. Nomura, A. Blazhev, J. Jolie, *et al.*, Phys. Rev. Lett. **108**, 062701 (2012), errata: **109**, 209904 and **114**, 189902.

[10] C. Sotty, M. Zielińska, G. Georgiev, D. L. Balabanski, A. E. Stuchbery, A. Blazhev, *et al.*, Phys. Rev. Lett. **115**, 172501 (2015).

[11] T. W. Hagen, A. Görgen, W. Korten, L. Grente, M.-D. Salsac, *et al.*, Phys. Rev. C **95**, 034302 (2017).

[12] K. Heyde and J. L. Wood, Rev. Mod. Phys. **83**, 1467 (2011).

[13] E. Clément, M. Zielińska, A. Görgen, W. Korten, S. Péru, *et al.*, Phys. Rev. Lett. **116**, 022701 (2016).

[14] E. Clément, M. Zielińska, *et al.*, Phys. Rev. C **94**, 054326 (2016).

[15] J.-M. Régis, J. Jolie, N. Saed-Samii, N. Warr, *et al.*, Phys. Rev. C **95**, 054319 (2017), erratum: **95**, 069902.

[16] F. Schussler, J. Pinston, E. Monnand, A. Moussa, G. Jung, and other, Nuclear Physics A **339**, 415 (1980).

[17] J. Park, A. B. Garnsworthy, R. Krücken, C. Andreoiu, G. C. Ball, P. C. Bender, A. Chester, A. Close, P. Finlay, P. E. Garrett, *et al.*, Phys. Rev. C **93**, 014315 (2016).

[18] F. Wohn, H. Mach, M. Moszyski, R. Gill, and R. Casten, Nuclear Physics A **507**, 141 (1990).

[19] H. Mach, M. Moszyn'ski, R. L. Gill, G. Molnár, F. K. Wohn, J. A. Winger, and J. C. Hill, Phys. Rev. C **41**, 350 (1990).

[20] C. Y. Wu, H. Hua, and D. Cline, Phys. Rev. C **68**, 034322 (2003).

[21] E. Clément, A. Görgen, W. Korten, E. Bouchez, A. Chatillon, J.-P. Delaroche, *et al.*, Phys. Rev. C **75**, 054313 (2007).

[22] N. Bree, K. Wrzosek-Lipska, A. Petts, A. Andreyev, B. Bastin, *et al.*, Phys. Rev. Lett. **112**, 162701 (2014).

[23] K. Sieja, F. Nowacki, K. Langanke, and G. Martínez-Pinedo, Phys. Rev. C **79**, 064310 (2009).

[24] T. Togashi, Y. Tsunoda, T. Otsuka, and N. Shimizu, Phys. Rev. Lett. **117**, 172502 (2016).

[25] T. Otsuka and Y. Tsunoda, Journal of Physics G: Nuclear and Particle Physics **43**, 024009 (2016).

[26] H. Abele, D. Dubbers, H. Häse, M. Klein, A. Knöpfler, M. Kreuz, T. Lauer, B. Märkisch, *et al.*, Nuclear Instruments and Methods in Physics Research Section A **562**, 407 (2006).

[27] J.-M. Régis, G. Simpson, A. Blanc, G. de France, M. Jentschel, U. Köster, P. Mutti, *et al.*, Nuclear Instruments and Methods in Physics Research Section A **763**, 210 (2014).

[28] W. Urban, M. Jentschel, B. Mrkisch, T. Materna, C. Bernards, C. Drescher, C. Fransen, J. Jolie, U. Köster, P. Mutti, T. Rzaca-Urban, and G. S. Simpson, Journal of Instrumentation **8**, P03014 (2013).

[29] P. Mutti, A. Blanc, G. de France, M. Jentschel, U. Köster, E. R. Martinez, G. Simpson, T. Soldner, C. A. Ur, and W. Urban, Advancements in Nuclear Instrumentation Measurement Methods and their Applications (ANIMMA) , 1 (2013).

[30] N. Saed-Samii, Diploma thesis (unpublished), Institute of Nuclear Pysics, cologne (2015).

[31] J.-M. Régis, G. Pascovici, J. Jolie, and M. Rudigier, Nuclear Instruments and Methods in Physics Research Section A **622**, 83 (2010).

[32] J.-M. Régis, H. Mach, G. Simpson, J. Jolie, G. Pascovici, N. Saed-Samii, N. Warr, *et al.*, Nuclear Instruments and Methods in Physics Research Section A **726**, 191 (2013).

[33] L. Bettermann, J.-M. Régis, T. Materna, J. Jolie, U. Köster, K. Moschner, and D. Radeck, Phys. Rev. C **82**, 044310 (2010).

[34] A. Smith, D. Patel, G. Simpson, R. Wall, J. Smith, O. Onakanmi, I. Ahmad, J. Greene, *et al.*, Physics Letters B **591**, 55 (2004).

[35] A. G. Smith, R. M. Wall, D. Patel, G. S. Simpson, D. M. Cullen, J. L. Durell, S. J. Freeman, *et al.*, Journal of Physics G: Nuclear and Particle Physics **28**, 2307 (2002).

[36] J. E. García-Ramos, K. Heyde, R. Fossion, V. Hellemans, and S. De Baerdemacker, The European Physical Journal A - Hadrons and Nuclei **26**, 221 (2005).